

# Density Functional Theory Study of Redox Pairs. 1. Dinuclear Iron Complexes That Undergo Multielectron Redox Reactions Accompanied by a Reversible Structural Change

Mu-Hyun Baik,<sup>†</sup> Tom Ziegler,<sup>‡</sup> and Cynthia K. Schauer<sup>\*,†</sup>

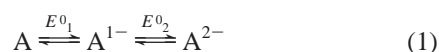
Contribution from the Department of Chemistry, University of North Carolina, Chapel Hill, North Carolina 27599-3290, and Department of Chemistry, University of Calgary, Calgary, Alberta, Canada T2N 1N4

Received September 30, 1999

**Abstract:** The single two-electron reduction for the Fe–Fe bonded dinuclear complexes  $\text{Fe}_2(\text{CO})_6(\mu_2\text{-PR}_2)_2$  ( $\text{R} = \text{CH}_3$ , **1-CH<sub>3</sub>**;  $\text{R} = \text{CF}_3$ , **1-CF<sub>3</sub>**) is studied by electronic structure calculations based on density functional theory (DFT) methods. Several theoretical models are evaluated, including gas-phase models and models that include solvation (COSMO model) and/or countercations. The experimentally observed cleavage of the Fe–Fe bond upon addition of electrons is reproduced in all calculations. The different theoretical models are evaluated by calculating the energy of the disproportionation reaction  $2\text{A}^- \rightarrow \text{A} + \text{A}^{2-}$  using the energies of the complexes  $[\mathbf{1-R}]^0$ ,  $[\mathbf{1-R}]^-$ , and  $[\mathbf{1-R}]^{2-}$ . As expected, gas-phase calculations poorly model the experimental redox behavior, and the inclusion of solvation or countercations is necessary to correctly predict that the disproportionation reaction is energetically downhill. The distribution of the added electrons over the molecules and the charge distribution as a function of alkali metal countercation ( $\text{Li}^+$ ,  $\text{Na}^+$ ,  $\text{K}^+$ ) are evaluated using the Hirshfeld charge analysis scheme. A qualitative correlation is found between the HOMO/LUMO energies of the redox species and the calculated redox potentials.

## Introduction

Molecules that undergo reversible two-electron redox processes observed at the same potential have attracted considerable attention,<sup>1</sup> and the fundamental aspects of the voltammetry in these systems have been investigated.<sup>2</sup> Typically, each sequential addition of an electron to a molecule becomes more difficult as a result of Coulombic repulsion. For the case of a two-electron reduction reaction (eq 1), as opposed to the



simultaneous addition of two electrons, such a reaction is attributed to two sequential one-electron reductions where the formal potential for adding the second electron,  $E_2^0$ , is more positive than the formal potential for adding the first electron,  $E_1^0$ .

For molecules that display  $2\text{e}^-$  redox behavior, the unfavorable electrostatic effects are overcome by structural rearrangements or chemical reactions that accompany the electron-transfer reactions.<sup>3</sup>

<sup>†</sup> University of North Carolina.

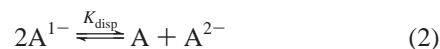
<sup>‡</sup> University of Calgary.

(1) (a) Bowyer, W. J.; Geiger, W. E. *J. Electroanal. Chem.* **1988**, 239, 253. (b) Evans, D. H.; Hu, K. *J. Chem. Soc., Faraday Trans.* **1996**, 92, 3983. (c) Evans, D. H.; Lehmann, M. W. *Acta Chem. Scand.* **1999**, 53, 765.

(2) (a) Polcyn, D. S.; Shain, I. *Anal. Chem.* **1966**, 38, 370. (b) Myers, R. L.; Shain, I. *Anal. Chem.* **1969**, 41, 980. (c) Richardson, D. E.; Taube, H. *Inorg. Chem.* **1981**, 20, 1278. (d) Hinkelmann, K.; Heinze, J. *Ber. Bunsen-Ges. Phys. Chem.* **1987**, 91, 243.

(3) Proton-coupled electron-transfer reactions, ligation reactions, and specific solvation reactions are examples of chemical reactions that give rise to multielectron redox behavior. See refs 1 and references therein.

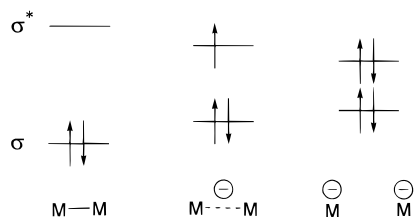
Bridged metal–metal bonded dinuclear complexes of general formulation  $[\text{L}_n\text{M}(\mu_2\text{-X})_2\text{ML}_n]^n$  represent a class of molecules that undergo a very simple structural change upon reduction.<sup>4</sup> The lowest unoccupied molecular orbital (LUMO) is M–M  $\sigma$ -antibonding, and sequential addition of two electrons to the LUMO results in stepwise cleavage of the M–M bond and an increase in the M–M bond distance by  $\sim 1.0 \text{ \AA}$  (Scheme 1). There are many examples of bridged dinuclear M–M bonded complexes that undergo reversible M–M bond cleavage and bond formation by either two sequential  $1\text{e}^-$  steps or a single apparent  $2\text{e}^-$  process.<sup>4–7</sup>



For a  $2\text{e}^-$  redox system, the disproportionation of the  $1\text{e}^-$  reduced intermediate (eq 2) is thermodynamically downhill, and the value of the disproportionation constant,  $K_{\text{disp}}$ , is related to the difference between the two  $1\text{e}^-$  potentials. The potential

(4) (a) Geiger, W. E.; Connelly, N. G. *Adv. Organomet. Chem.* **1985**, 24, 87. (b) Gennett, T.; Geiger, W. E.; Willett, B.; Anson, F. C. *J. Electroanal. Chem.* **1987**, 222, 151.

(5) For examples of electrochemical studies of dinuclear M–M bonded complexes that display  $2\text{e}^-$  redox behavior, see the following: (a) Dessy, R. E.; Weissman, P. M.; Pohl, R. L. *J. Am. Chem. Soc.* **1966**, 88, 5117. (b) Dessy, R. E.; Kornman, R.; Smith, C.; Haytor, R. *J. Am. Chem. Soc.* **1968**, 90, 2001. (c) Dessy, R. E.; Rheingold, A. L.; Howard, G. D. *J. Am. Chem. Soc.* **1972**, 94, 746. (d) Collman, J. P.; Rothrock, R. K.; Finke, R. G.; Moore, E. J.; Rose-Munch, F. *Inorg. Chem.* **1982**, 21, 146. (e) Ginsburg, R. E.; Rothrock, R. K.; Finke, R. G.; Collman, J. P.; Dahl, R. L. *J. Am. Chem. Soc.* **1979**, 101, 6550. (f) Fernandes, J. B.; Zhang, L. Q.; Schultz, F. A. *J. Electroanal. Chem.* **1991**, 297, 145. (g) Smith, D. A.; Zhung, B.; Newton, W. E.; McDonald, J. W.; Schultz, F. A. *Inorg. Chem.* **1987**, 26, 2524. (h) DiMaio A. J.; Rheingold A. L.; Chin T. T.; Pierce D. T.; Geiger, W. E. *Organometallics* **1998**, 17, 1169. (i) Chin, T. T.; Geiger, W. E.; Rheingold, A. L. *J. Am. Chem. Soc.* **1996**, 118, 5002.

**Scheme 1.** Schematic MO Diagram of the Redox Process

for the  $2 e^-$  wave,  $E_{1/2}$ , is observed at the average of the two  $e^-$  potentials:<sup>2</sup>

$$E_{1/2} = \frac{E_1^0 + E_2^0}{2} \quad (3)$$

$$\Delta E_{1/2} = E_2^0 - E_1^0 = \frac{RT}{F} \ln K_{\text{disp}} \quad (4)$$

The factors that dictate a single  $2 e^-$  redox step versus two  $1 e^-$  redox steps in these systems are not readily apparent.<sup>8</sup>

We report results from electronic structure calculations based on density functional theory (DFT)<sup>9</sup> for the bridged  $2 e^-$  redox system,  $[\text{Fe}_2(\text{CO})_6(\mu_2\text{-PR}_2)_2]^{0/-2-}$ .<sup>5a-e</sup> The energy of the disproportionation reaction (eq 2) is evaluated on the basis of the calculated results as an estimate of the disproportionation free energy.<sup>10</sup> An accurate calculation of the energy of the disproportionation reaction is a very demanding problem. The species involved in the disproportionation reaction have different structures and different charges, and the monoanion has an unpaired spin (triplet), while the neutral and dianionic species are singlets.<sup>5c</sup> Further, solvation will have a pronounced influence on the energies of charged species.<sup>11</sup> All of these factors need to be accurately represented to correctly predict the relative energies of the three species. The results of gas-phase models and of models that include countercations and/or solvation are presented. The results from different models are evaluated by examining the energy of the disproportionation reaction.

**Computational Details/Theoretical Methods**

Two DFT program packages were used: Amsterdam Density Functional program ADF 1999 and DMol 960. ADF, developed by

(6) For examples of coupled chemical reactions giving rise to  $2 e^-$  behavior in dinuclear M–M bonded systems, see: (a) Gaudiello, J. G.; Wright, T. C.; Jones, R. A.; Bard, A. J. *J. Am. Chem. Soc.* **1985**, *107*, 888. (b) Mann, K. R.; Rhodes, M. R. *Inorg. Chem.* **1984**, *23*, 2053. (c) Hill, M. G.; Mann, K. R. *Inorg. Chem.* **1991**, *30*, 1431. (d) Tommasino, J. B.; de Montauzon, D.; He, X.; Maisonnat, A.; Poilblanc, R.; Verpeaux, J. N.; Amatore, C. *Organometallics* **1992**, *11*, 4150. (e) Moulton, R.; Weidman, T. W.; Vollhardt, K. P. C.; Bard, A. J. *Inorg. Chem.* **1986**, *25*, 1846. (f) Bond, A. M.; Colton, R.; Jackowski, J. J. *Inorg. Chem.* **1978**, *17*, 2153.

(7) Our interest in the two-electron redox problem was stimulated by our discovery of a series of triangular iron clusters,  $\text{Fe}_3(\text{CO})_9(\mu_3\text{-EML}_n)_2$ , (E = P, As, Sb;  $\text{ML}_n = \text{Cr}(\text{CO})_5$ ,  $\text{MnCp}(\text{CO})_2$ ) that display a single two-electron reduction accompanied by cleavage of an Fe–Fe bond. (a) Bautista, M. T.; White, P. S.; Schauer, C. K. *J. Am. Chem. Soc.* **1991**, *113*, 8963. (b) Koide, Y.; Bautista, M. T.; White, P. S.; Schauer, C. K. *Inorg. Chem.* **1992**, *31*, 3690. (c) Koide, Y.; Schauer, C. K. *Organometallics* **1993**, *12*, 4854. (d) Collins, B. E.; Koide, Y.; Schauer, C. K.; White, P. S. *Inorg. Chem.* **1997**, *36*, 6172.

(8) Simple qualitative arguments presented in the literature have suggested that the  $2 e^-$  redox behavior in M–M bonded systems is dictated by the fact that the HOMO energy is lowered in the intermediate species,  $\text{A}^-$ . Therefore,  $\text{A}^-$  accepts a second electron at a lower potential. The lowering of the HOMO is a common feature for any system that undergoes M–M bond cleavage upon adding electrons and is only one factor that impacts the relative energy of  $\text{A}^-$ .

(9) (a) Parr, R. G.; Yang, W. *Density Functional Theory of Atoms and Molecules*; Oxford University Press: New York, 1989. (b) Ziegler, T. *Chem. Rev.* **1991**, *91*, 651. (c) Baerends, E. J.; Gritsenko, O. V. *J. Phys. Chem. A* **1997**, *101*, 5382.

Baerends et al.,<sup>12</sup> utilizes Slater-type orbitals (STO) as the basis set. DMol, developed by Delley et al.,<sup>13</sup> uses a numerical basis set. Unrestricted spin-treatment was utilized for all calculations. Vibrational frequency calculations, which are very desirable to confirm that the optimized geometries are truly minimum structures, were only carried out for the **1-CH<sub>3</sub>** series. However, the good correlation of the optimized structures to crystal structures of the neutral and dianionic forms, together with the fact that the observed structural change primarily involves the Fe–Fe vector, supports the fact that our optimized structures are physically significant.

**DMol.** The local exchange-correlation potential, as suggested by Vosko, Wilk, and Nuisair<sup>14a</sup> (VWN), augmented by Becke's 1988 version<sup>14b</sup> of the gradient-corrected exchange functional, and the Perdew and Wang correlation functional<sup>14c</sup> were employed for the full geometry optimization using the DMol 960 program package. A set of "double numerical plus" (DNP) basis functions with a FINE mesh was used throughout the study, and all electrons were included (no frozen core).

**ADF.** In the ADF calculations, the triple- $\zeta$  STO basis set was utilized, with one set of polarization functions as provided in the package (Basis Set IV, comparable to 6-311G\*), together with the VWN local exchange-correlation potential, augmented by exchange and correlation functionals as suggested by Perdew and Wang (PW91).<sup>14d</sup> The inner core shells were always treated by the frozen core approximation.

For a few selected cases, we have repeated the calculation using the Becke-88 exchange and Lee–Yang–Parr<sup>14e</sup> correlation functional (BLYP). Good agreement was found with the PW91 results, and the geometries optimized using PW91 compare slightly better with experimental values.

**COSMO.** Solvation effects have been included using the conductor-like screening model (COSMO) suggested by Klamt and Schüürmann<sup>15a</sup> and implemented in DMol by Andzelm and Klamt et al.<sup>15b</sup> and in ADF by Pye and Ziegler.<sup>15c</sup> The crucial part of the solvation calculation is the choice of radii that define the cavity representing the solute. In DMol calculations, the Klamt surface was used, whereas in ADF calculations, the solvent-excluding surface was chosen. The standard radii provided with the package were used in DMol calculations (Fe, 1.95 Å; P, 1.75 Å; C, 1.53 Å; O, 1.36 Å; H, 1.08 Å; F, 1.30 Å; Li, 1.22 Å; Na, 2.20 Å; K, 2.39 Å). Due to its recent implementation, standard COSMO radii for ADF are not routinely available. The radii

(10) For reports of calculating redox potentials using ab initio methods, see: (a) Wheeler, R. A. *J. Am. Chem. Soc.* **1994**, *116*, 11048. (b) Boesch, S. E.; Grafton, A. K.; Wheeler, R. A. *J. Phys. Chem.* **1996**, *100*, 10083. (c) Raymond, K. S.; Grafton, A. K.; Wheeler, R. A. *J. Phys. Chem. B* **1997**, *101*, 623. (d) Moock, K. H.; Macgregor, S. A.; Heath, G. A.; Derrick, S.; Boere, R. T. *J. Chem. Soc., Dalton Trans.* **1996**, 2067. (e) Macgregor, S. A.; Moock, K. H. *Inorg. Chem.* **1998**, *37*, 3284. (f) DiLabio, G. A.; Pratt, D. A.; LoFaro, A. D.; Wright, J. S. *J. Phys. Chem. A* **1999**, *103*, 1653. (g) Li, J.; Fisher, C. L.; Chen, J. L.; Bashford, D.; Noodleman, L. *Inorg. Chem.* **1996**, *35*, 4694. (h) Konecny, R.; Li, J.; Fisher, C. L.; Dillet, B.; Bashford, D.; Noodleman, L. *Inorg. Chem.* **1999**, *38*, 940. (i) Li, J.; Nelson, M. R.; Peng, C. Y.; Bashford, D.; Noodleman, L. *J. Phys. Chem. A* **1998**, *102*, 6311. (j) Li, J.; Fisher, C. L.; Konecny, R.; Bashford, D.; Noodleman, L. *Inorg. Chem.* **1999**, *38*, 929. (k) Mouesca, J.-M.; Chen, J. L.; Noodleman, L.; Bashford, D.; Case, D. A. *J. Am. Chem. Soc.* **1994**, *116*, 11898. (l) Winget, P.; Weber, E. J.; Cramer, C. J.; Truhlar, D. G. *Phys. Chem. Chem. Phys.* **2000**, *2*, 1231. (m) Kettle, L. J.; Bates, S. P.; Mount, A. R. *Phys. Chem. Chem. Phys.* **2000**, *2*, 195. (n) Reynolds, C. A. *Int. J. Quantum Chem.* **1995**, *56*, 677.

(11) Bockris, J. O'M.; Reddy, A. K. N. *Modern Electrochemistry, Volume 1, Ionics*, 2nd ed.; Plenum Press: New York, 1998.

(12) (a) ADF 1999; Vrije Universiteit Amsterdam: Amsterdam, The Netherlands, 1999. (b) Baerends, E. J.; Ellis, D. E.; Ros, P. *Chem. Phys.* **1973**, *2*, 41. (c) te Velde, G.; Baerends, E. J. *J. Comput. Phys.* **1992**, *99*, 84. (d) Fonseca Guerra, C.; et al. *METECC-95* **1995**, 305.

(13) (a) Delley, B. *Chem. Phys. Lett.* **1986**, *110*, 329. (b) Delley, B. *J. Chem. Phys.* **1990**, *92*, 508. (c) Molecular Simulations Inc., San Diego, CA.

(14) (a) Vosko, S. H.; Wilk, L.; Nusair, M. *Can. J. Phys.* **1980**, *58*, 1200. (b) Becke, A. D. *Phys. Rev. A* **1988**, *38*, 3098. (c) Perdew, J. P.; Wang, Y. *Phys. Rev. B* **1992**, *45*, 13244. (d) Perdew, J. P.; et al. *Phys. Rev. B* **1992**, *46*, 6671. (e) Lee, C.; Yang, W.; Parr, R. G. *Phys. Rev. B* **1988**, *37*, 786.

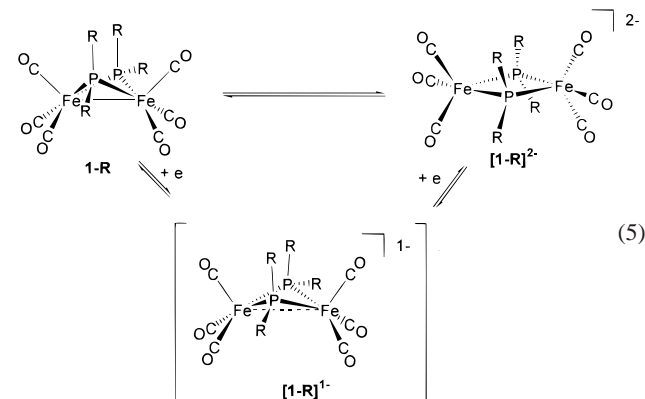
(15) (a) Klamt A.; Schüürmann, G. *J. Chem. Soc., Perkin Trans.* **1993**, *2*, 799. (b) Andzelm, J.; Kölmel, C.; Klamt, A. *J. Chem. Phys.* **1995**, *103*, 9312. (c) Pye, C. C.; Ziegler, T. *Theor. Chem. Acc.* **1999**, *101*, 396.

suggested by Pye and Ziegler<sup>15c</sup> were used, which are based on the COSMO implementation by Truong and Stefanovich<sup>16</sup> for the GAUSSIAN 92 package. Radii were estimated for the transition metals, for which no data were available (Fe, 2.40 Å; P, 2.40 Å; C, 2.30 Å; O, 1.40 Å; H, 1.16 Å; F, 1.423 Å; Li, 1.50 Å; Na, 2.71 Å; K, 2.95 Å). A direct comparison of the calculated absolute solvation energies is problematic if different surfaces and radii are used in addition to different charge distribution schemes. Since the metal is mostly inside the cavity, the approximate character of the metal radius is not a significant source of error. For charged species, the dominant term is the monopole term inside the surface, and the sphere sizes are less important. Only a moderate agreement of the solvation energies between the two DFT packages is expected. The dielectric constant of acetonitrile (37.5) was used to mimic a common solvent for electrochemical experiments. In ADF calculations, the quantity  $x$  in the scaling factor  $(\epsilon - 1)/(\epsilon + x)$  is set equal to zero.

## Results and Discussion

**Overview.** The initial system chosen for our study is based on the dinuclear phosphido-bridged  $\text{Fe}_2\text{P}_2$  core. The substituents bound to the phosphido group present the opportunity to remotely tune the electronic structure of the complex and examine the impact on the electronic structure of the neutral, monoanion, and dianion species. Experimentally, the two-electron redox chemistry of the phenyl (Ph)<sup>5d,e</sup> and methyl (Me)<sup>5a,b</sup> derivatives is well-established, and structural results are available for several different members of the series, including  $\mathbf{1-CF}_3$ ,<sup>17</sup>  $\mathbf{1-CH}_3$ ,<sup>17</sup> and  $[\mathbf{1-Ph}]^{2-}$ .<sup>5c</sup>

The diironbisphosphido-bridged complexes have been examined using approximate theoretical methods by Burdett<sup>18a</sup> (extended Hückel MO calculation) and Dahl, Fenske, and co-workers<sup>18b</sup> (Fenske–Hall method). A qualitative understanding



of the process leading to the structural change that accompanies the redox reaction can be derived from very simple considerations. The LUMO of this 34-electron dinuclear complex is Fe–Fe antibonding in character. Occupation of the LUMO leads to a reduction in the Fe–Fe bond order, and elongation of the Fe–Fe distance. Addition of a second electron to the singly occupied orbital results in a further elongation of the Fe–Fe bond. Figure 1 shows 3-D plots of the orbitals directly involved in the redox process from the results of Fenske–Hall calculations.<sup>19</sup>

For approximate methods, idealized geometries from crystal structures are used in the calculations, and the chemically interesting question of how the reduction changes the structure

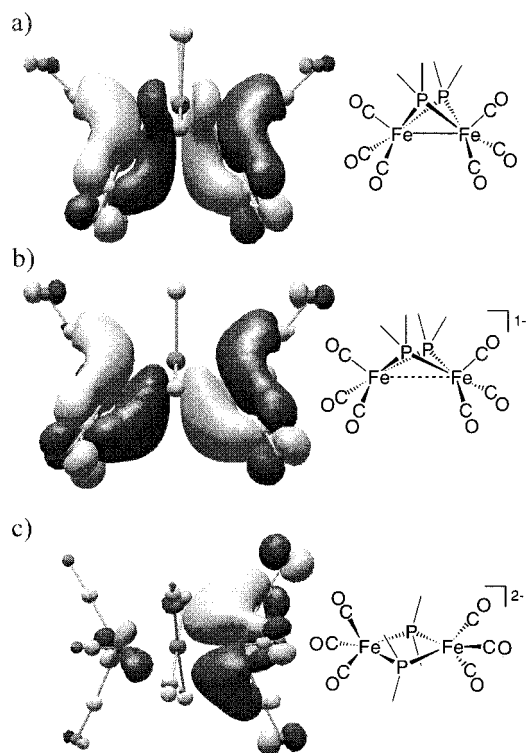


**Figure 1.** LUMO (a), SOMO (b) and HOMO (c) of  $\mathbf{1-CH}_3$ ,  $[\mathbf{1-CH}_3]^-$ , and  $[\mathbf{1-CH}_3]^{2-}$ , respectively, from Fenske–Hall molecular orbital calculations.

and the charge distribution is unaddressable. Our approach to understanding the electrochemistry of organometallic complexes in terms of electronic structure changes relies on the assumption that the free energy change for the disproportionation reaction is dominated by the changes in bonding and electronic structure, together with electrostatic interaction of the solute with the dielectric solvent. The interactions of the complex with solvent molecules are not treated explicitly; therefore, purely solvent-based contributions to the redox enthalpy such as specific interactions of individual solvent molecules and solvent reorganization energies are neglected.

Below we present the results of calculations for the  $[\mathbf{1-R}]^{0/-2-}$  system directed at addressing the change in electronic structure upon reduction. Initially, the results from gas-phase calculations will be presented, with an emphasis on comparing the calculated structures to the experimentally determined ones. Second, the impact of including solvation will be described, and a detailed analysis of how the charge is distributed over the molecule during the reduction reaction. Third, ion pair formation is allowed in gas-phase and the solvated model. These results in total provide a protocol for evaluating energies of species involved in electrochemical reactions.

**1. Theoretical Models.** DFT methods have been used extensively for inorganic problems, and the accuracy of the calculated energies has been demonstrated for various systems, including organometallic complexes.<sup>20</sup> To avoid misinterpretations of numerical results that are due to computational implementations, we have carried out all the calculations using both the ADF and DMol packages.

**1.1. Gas-Phase Structures.** The initial question to be addressed is if the experimentally observed structural changes with addition of electrons are reproduced by the DFT method.

(16) Truong, T. N.; Stefanovich, E. V. *Chem. Phys. Lett.* **1995**, *240*, 253.

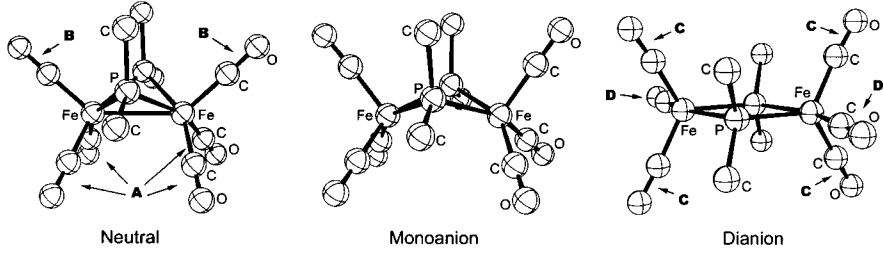
(17) Clegg, W. *Inorg. Chem.* **1976**, *15*, 1609.

(18) (a) Burdett, J. K. *J. Chem. Soc., Dalton Trans.* **1977**, 423. (b) Teo, B. K.; Hall, M. B.; Fenske, R. F.; Dahl, L. F. *Inorg. Chem.* **1975**, *16*, 3103.

(19) (a) Hall, M. B.; Fenske, R. F. *Inorg. Chem.* **1972**, *11*, 768. (b) Fenske, R. F. *Pure Appl. Chem.* **1971**, *27*, 61.

(20) (a) See references given in ref 9b. (b) For a summary of recent studies of transition metal complexes by DFT, see: Mire, L. W.; Wheeler, S. D.; Wagenseller, E.; Marynick, D. S. *Inorg. Chem.* **1998**, *37*, 3099.



**Table 1.** Selected Bond Lengths and Angles of  $[\text{Fe}_2(\text{CO})_6(\mu_2\text{-PR}_2)_2]$ ,  $[\text{Fe}_2(\text{CO})_6(\mu_2\text{-PR}_2)_2]^-$ , and  $[\text{Fe}_2(\text{CO})_6(\mu_2\text{-PR}_2)_2]^{2-}$ <sup>a</sup>


	R = CH <sub>3</sub>							R = CF <sub>3</sub>							R = Ph exptl
	exptl	DMol	DMol	DMol	ADF	ADF	ADF	exptl	DMol	DMol	DMol	ADF	ADF	ADF	
charge	<b>0</b>	0	-1	-2	0	-1	-2	<b>0</b>	0	-1	-2	0	-1	-2	<b>-2</b>
Fe-Fe/Å	<b>2.665</b>	2.722	3.282	3.717	2.711	3.290	3.741	<b>2.819</b>	2.804	3.388	3.689	2.801	3.471	3.710	<b>3.630</b>
Fe-P/Å	<b>2.209</b>	2.251	2.284	2.325	2.244	2.285	2.330	<b>2.193</b>	2.245	2.277	2.304	2.240	2.278	2.308	<b>2.288</b>
Fe-P'/Å		2.248	2.285	2.297	2.240	2.280	2.310		2.230	2.273	2.266	2.232	2.274	2.265	<b>2.271</b>
P-P'/Å	<b>2.925</b>	2.989	2.863	2.749	2.974	2.850	2.746	<b>2.921</b>	2.979	2.835	2.689	2.946	2.815	2.669	<b>2.759</b>
flap angle <sup>17</sup> /deg	<b>107.3</b>	108.1	134.4	179.1	107.8	134.6	179.3	<b>118.9</b>	114.2	144.3	172.7	112.7	152.1	177.4	<b>180.0</b>
Fe-P-Fe/deg	<b>74.2</b>	74.5	91.8	107.0	74.4	92.2	107.4	<b>80.0</b>	77.6	96.2	107.6	77.6	99.4	108.5	<b>105.5</b>
P-Fe-P/deg	<b>82.9</b>	83.2	77.5	73.0	83.1	77.2	72.5	<b>83.5</b>	83.5	77.1	72.1	82.4	76.4	71.4	<b>74.5</b>
C-P-C/deg		98.7	97.4	96.3	98.4	97.3	96.1	<b>96.6</b>	96.4	94.0	93.9	95.7	94.0	93.1	<b>101.0</b>
<i>E</i> (binding)/eV		-153.98	-155.60	-154.54	-205.54	-207.20	-206.13		-162.95	-166.02	-166.19	-209.43	-212.55	-212.64	
<i>E</i> (LUMO)/eV		-3.26	0.95	4.25	-2.85	1.36	4.63		-4.69	-0.40	3.17	-4.41	-0.21	3.39	
<i>E</i> (HOMO)/eV		-5.96	-0.55	2.08	-5.57	-0.25	2.46		-6.98	-1.97	1.12	-6.73	-1.93	1.36	

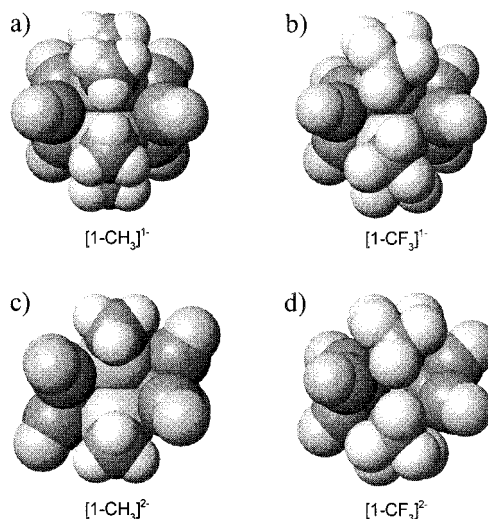
<sup>a</sup> Hydrogens on the methyl groups are omitted for clarity. Structurally related carbonyl sites are labeled using the letters A, B, C, and D. Experimental values are taken from refs 1b and 10.

Selected bond lengths and angles of the calculated structures are compared with the available crystal structure data<sup>5e,17</sup> in Table 1. The structure of the experimentally unisolable monoanionic species is calculated by starting from the fully optimized neutral geometry and defining a negative charge. Other than the charge, no further information is provided, and no symmetry restrictions are employed. The procedure is repeated for the dianionic form using the optimized monoanionic geometry as a starting point.

The calculated Fe-Fe distances of 2.71 Å (ADF)/2.72 Å (DMol) for neutral **1-CH<sub>3</sub>** are slightly longer than the experimental distance of 2.665 Å. The optimized Fe-Fe distance for the monoanion 3.29 Å (ADF) is reasonable for a singly reduced intermediate, although there is no experimental comparison. The Fe<sub>2</sub>P<sub>2</sub> core of the dianion has a planar structure, and the final Fe-Fe distance of 3.74 Å (ADF) indicates that there is no metal-metal bonding in the dianion. Dahl et al.<sup>5e</sup> have isolated the [Na(2,2,2-crypt)] salt of the phenyl-substituted analogue **[1-Ph]<sup>2-</sup>** and found an Fe-Fe distance of 3.630 Å in the planar dianion.

Burdett<sup>18a</sup> and Clegg<sup>17</sup> studied the structural change of the dinuclear neutral complexes **1-R** (R = CH<sub>3</sub>, CF<sub>3</sub>, Ph, H) as a function of the R substituent. They found that the Fe-Fe distance increases if the CH<sub>3</sub> group is replaced by the more electronegative CF<sub>3</sub> group. The more electronegative R group gives rise to a larger p-character of the P-R bond, leading to a smaller R-P-R angle. The longer Fe-Fe distance and larger flap angle<sup>21</sup> Fe-P-P-Fe follow from the larger s-character for the P-Fe bond. The experimentally observed increase in the Fe-Fe distance to 2.82 Å upon replacement of the CH<sub>3</sub> group by the CF<sub>3</sub> group is reproduced in both ADF and DMol calculations for **1-CF<sub>3</sub>**.

In the first reduction step, the Fe-Fe distance increases by 0.58 Å (ADF)/0.56 Å (DMol) in **1-CH<sub>3</sub>**. Addition of a second electron increases the Fe-Fe distance by an additional 0.45 Å (ADF)/0.43 Å (DMol). In **1-CF<sub>3</sub>**, the structural change is partitioned differently over the two one-electron steps. The first

**Figure 2.** Space-filling models of the monoanionic and dianionic complexes.

reduction results in an Fe-Fe distance increase of 0.67 Å (ADF)/0.58 Å (DMol), and the second electron causes a displacement of 0.24 Å (ADF)/0.30 Å (DMol). The addition of the first electron might be expected to give rise to a larger elongation of the Fe-Fe bond due to steric crowding of the CR<sub>3</sub> ligands in the neutral form, which is relieved in the monoanionic structure. This expectation is consistent with the larger Fe-Fe bond elongation observed for **1-CF<sub>3</sub>** in the first step. Space-filling models of the mono- and dianionic forms of **1-CH<sub>3</sub>** and **1-CF<sub>3</sub>** are compared in Figure 2. In **[1-CH<sub>3</sub>]<sup>-</sup>** (Figure 2a), the methyl groups are small enough to fit between the metal sites without any steric perturbation of the carbonyl ligand orientation. The CF<sub>3</sub> analogue (Figure 2b) shows a slight distortion from C<sub>2v</sub> symmetry, arising from a rotation of the CF<sub>3</sub> groups to avoid the repulsive (both steric and electrostatic) interaction. The steric tension is relieved efficiently in the dianionic form (Figure 2c,d) by the structure adopting a planar geometry. The final Fe-Fe distance is mainly determined by

(21) The term "flap angle" refers to the Fe-P-P-Fe dihedral angle.

minimizing the Fe–Fe antibonding interaction, which is achieved at a distance of 3.7 Å in the planar Fe<sub>2</sub>P<sub>2</sub> structure.

Calculations on the dianions show that the Kohn–Sham orbital energies of a few of the occupied orbitals are positive. We have systematically changed the input parameters (exchange–correlation functional, computational accuracy, and basis sets) using both ADF and DMol to exclude purely numerical effects. All attempts gave positive HOMO energies, suggesting that the removal of the electron from the molecule is energetically downhill.<sup>22–24</sup> Single-point calculations using the optimized geometry of [1-CH<sub>3</sub>]<sup>2-</sup> with a single negative charge confirm that the removal of one electron is energetically downhill by 0.38 eV (ADF) and 0.39 eV (DMol). Two interpretations of this results are possible: (a) The exchange–correlation functionals used are unable to give a correct description of the dianion, and the unbound electron is the result of imperfections of the computational method. (b) The dianion is unstable with respect to electron loss in the gas phase and is truly an unstable species.

**1.2. Gas-Phase Disproportionation Energies.** The disproportionation reaction (eq 2) involves two half-reactions:



The energy difference between the neutral and monoanion,  $\Delta E_1$ , is the adiabatic ionization energy of the monoanion including structural relaxation (eq 6). The value  $\Delta E_2$  (eq 7) is the adiabatic electron attachment energy of the monoanion including structural relaxation and is given by the energy difference between the dianion and monoanion. The total energy balance for the disproportionation is

$$\begin{aligned} \Delta\Delta E &= \Delta E_1 + \Delta E_2 \\ &= [E(A) - E(A^-)] + [E(A^{2-}) - E(A^-)] \end{aligned} \quad (8)$$

A negative  $\Delta\Delta E$  value indicates an energetically downhill disproportionation reaction, while a positive  $\Delta\Delta E$  value indicates that the disproportionation is uphill.

It is convenient to consider binding energies<sup>25</sup> instead of total energies, where the binding energy is generally defined as the

(22) (a) Jarecki, A. A.; Davidson, E. R. *Chem. Phys. Lett.* **1999**, *300*, 44. (b) Galbraith, J. M.; Schaefer, H. F. *J. Chem. Phys.* **1996**, *105*, 862. (c) Rösch N.; Trickey, S. B. *J. Chem. Phys.* **1997**, *106*, 8940. (d) Schwarz, K. *Chem. Phys. Lett.* **1978**, *57*, 605. (e) J. F. Janak, *Phys. Rev. B* **1978**, *18*, 7165.

(23) Van Leeuwen and Baerends have proposed a functional (LB94) with a correct long-range behavior and have shown that the typical errors of HOMO eigenvalues (ref 24), which might be as large as 5 eV, can be corrected efficiently by using this new functional. Using the LB94 functional on the PW91-optimized geometry, a negative HOMO eigenvalue (–2.70 eV) is obtained. This result provides an argument that the unbound electron may arise from the wrong long-range behavior of the commonly available functionals. Unfortunately, the short-range behavior of the LB94 functional gives rise to inaccurate binding energies, so that the evaluation of the relative stabilities on the basis of LB94-binding energies of the three species is not recommended.

(24) van Leeuwen, R.; Baerends, E. *J. Phys. Rev. A* **1994**, *49*, 2421.

(25) The definition of binding energy differs slightly in the two DFT packages used. In ADF calculations, atomic calculations are carried out by treating the atoms as spin-restricted symmetric objects, which leads to a description of the atoms that does not correspond to the correct multiplet state. DMol carries out a full atomic calculation using the parameters defined for the molecule. The energies formally assigned to the atoms in ADF are therefore higher than those in DMol. Since binding energy is defined as the total molecular energy minus the sum of atomic energies, DMol and ADF binding energies are shifted by a constant value for a given composition of the molecule. The two conventions of reference energies will afford the same energy differences for processes in which no bond is broken. For bond dissociation energies appropriate corrections are added to the ADF atomic energies to obtain the correct bond dissociation energies.

**Table 2.** Binding Energy Differences of the Gas-Phase Calculation, in eV

	(1-) → (0)	(1-) → (2-)	total
DMol, 1-CH <sub>3</sub>	1.62	1.06	2.68
DMol, 1-CF <sub>3</sub>	3.07	-0.16	2.90
ADF, 1-CH <sub>3</sub>	1.66	1.07	2.73
ADF, 1-CF <sub>3</sub>	3.12	-0.09	3.04

total molecular energy minus the sum of atomic energies. If the energetics of the redox reaction are mainly determined by changes in the electronic structure arising from the structural change,<sup>26,27</sup> then the total reaction enthalpy for the two-electron process should be dominated by the  $\Delta\Delta E$  that is calculated on the basis of the electronic changes. The difference in the binding energies between the monoanion and dianion should be larger than that of the monoanion and neutral species for the disproportionation reaction to give a net stabilization. Table 2 summarizes  $\Delta\Delta E$  values for the gas-phase model. The calculated  $\Delta\Delta E$  values of approximately 2.7 eV (62 kcal/mol; ADF) and 3.0 eV (70 kcal/mol; DMol) indicate that the disproportionation reaction is energetically uphill. These  $\Delta\Delta E$  values are orders of magnitude too high for a redox equilibrium. A similar energy profile was reported by Dewar et al.<sup>28</sup> in their gas-phase study of the neutral, monoanion, and dianion of cyclooctatetraene. The failure of gas-phase models to correctly predict the relative energies of species with different charges is not surprising. Solvation is expected to have a pronounced impact on the energetics of the system.<sup>11,27</sup> Hu and Evans<sup>30</sup> have demonstrated that theoretical methods (AM1) can be used to study 2 e<sup>-</sup> redox reactions qualitatively, if solvation is included by estimating its magnitude using the Born treatment of ionic solvation.

(26) The energy of the disproportionation reaction calculated from results of an electronic structure calculation is a measure of the 0 K enthalpy of reaction. An electrochemical experiment measures the free energy of disproportionation at 298 K; therefore, an exact calculation of the free energy of the disproportionation reaction requires inclusion of solvation free energy (the dominant contribution) together with changes in zero-point energy and intramolecular entropy. The COSMO solvation model employed herein is a continuum model that is parametrized for the solvation free energy. For the system [Fe<sub>2</sub>(CO)<sub>6</sub>(μ<sub>2</sub>-PMe<sub>2</sub>)<sub>2</sub>]<sup>0/-2-</sup>, a demanding full vibrational calculation was carried out to assess the magnitude of the changes in zero-point energy and intramolecular vibrational entropy. The zero-point energy correction to the disproportionation free energy was +0.05, and the intramolecular vibrational correction was +0.02 V. Therefore, errors of less than 100 mV are expected from neglecting these contributions. The electronic contribution to entropy is expected to be smaller than the vibrational entropy (refs 27a–c). Details of the zero-point energy and vibrational calculations are given in the Supporting Information.

(27) The work of Richardson et al. delineates the factors in the thermochemical interpretation of electrode potentials for transition metal complexes in terms of bond energies, entropy changes, and solvation energies. Gas-phase free energies of ionization measured using the electron-transfer equilibrium technique can be combined with electrochemical data to extract the differential solvation energy for a redox pair. (a) Richardson, D. E. *Inorg. Chem.* **1990**, *29*, 3213. (b) Richardson, D. E.; Sharpe, P. *Inorg. Chem.* **1991**, *30*, 1412. (c) Richardson, D. E.; Sharpe, P. *Inorg. Chem.* **1993**, *32*, 1809. (d) Richardson, D. E.; Lang, L.; Eyley, J. R.; Kircus, S. R.; Zheng, X.; Morse, C. A.; Hughes, R. P. *Organometallics* **1997**, *16*, 149. (e) Richardson, D. E.; Ryan, M. F.; Geiger, W. E.; Chin, T. T.; Hughes, R. P.; Curnow, O. J. *Organometallics* **1993**, *12*, 613. (f) Richardson, D. E.; Ryan, M. F.; Khan, N. I.; Maxwell, K. A. *J. Am. Chem. Soc.* **1992**, *114*, 10482. (g) Sharpe, P.; Richardson, D. E. *J. Am. Chem. Soc.* **1991**, *113*, 8339. (h) Sharpe, P.; Alameddini, G.; Richardson, D. E. *J. Am. Chem. Soc.* **1994**, *116*, 11098. (i) Ryan, M. F.; Eyley, J. R.; Richardson, D. E. *J. Am. Chem. Soc.* **1992**, *114*, 8611. (j) Ryan, M. F.; Richardson, D. E.; Lichtenberger, D. L.; Gruhn, N. E. *Organometallics* **1994**, *13*, 1190.

(28) (a) Dewar, M. J. S.; Harget, A.; Haselbach, E. *J. Am. Chem. Soc.* **1969**, *91*, 7521. (b) Zuilhof, H.; Lodder, G. *J. Phys. Chem.* **1995**, *99*, 8033.

(29) We have investigated the electrochemical behavior of cyclooctatetraene using the same procedure presented here. These results will be published in the second part of this series of theoretical studies.

(30) (a) Hu, K.; Evans, D. H. *J. Phys. Chem.* **1996**, *100*, 3030. (b) Evans, D. H.; Hu, K. *J. Chem. Soc., Faraday Trans.* **1996**, *92*, 3983.

**Table 3.** COSMO Geometries and Binding Energies

	R = CH <sub>3</sub>						R = CF <sub>3</sub>					
	DMol	DMol	DMol	ADF	ADF	ADF	DMol	DMol	DMol	ADF	ADF	ADF
charge	0	-1	-2	0	-1	-2	0	-1	-2	0	-1	-2
Fe-Fe'/Å	2.708	3.235	3.690	2.708	3.277	3.719	2.807	3.371	3.671	2.801	3.469	3.701
Fe-P/Å	2.260	2.293	2.329	2.255	2.291	2.332	2.238	2.273	2.297	2.242	2.277	2.300
Fe-P'/Å	2.255	2.293	2.302	2.251	2.284	2.308	2.227	2.266	2.260	2.234	2.272	2.265
P-P'/Å	2.999	2.913	2.797	2.983	2.867	2.776	2.968	2.844	2.690	2.950	2.814	2.672
flap angle <sup>17</sup> /deg	106.7	132.0	180.0	106.6	133.6	179.7	114.6	144.7	172.7	112.7	152.2	177.4
Fe-P-Fe/deg	73.7	89.7	105.7	73.9	91.5	106.5	77.9	95.9	107.3	77.5	99.4	108.3
P-Fe-P/deg	83.2	78.9	74.3	82.9	77.6	73.4	83.3	77.6	72.6	82.5	76.4	71.6
C-P-C/deg	99.3	98.6	97.8	98.3	97.4	96.2	96.3	94.6	94.0	95.8	94.1	92.7
E(binding)/eV	-154.45	-157.34	-160.65	-205.57	-208.49	-211.65	-163.45	-167.34	-171.55	-209.29	-213.15	-217.55
E(LUMO)/eV	-2.91	-1.87	-1.62	-2.92	-1.69	-1.36	-4.05	-2.96	-2.22	-4.41	-2.52	-2.46
E(HOMO)/eV	-5.70	-3.35	-3.99	-5.66	-3.30	-3.64	-6.35	-4.55	-4.35	-6.72	-5.08	-4.53
electrostatic $E_{\text{sol}}/$ kcal mol <sup>-1</sup>	-11.35	-40.02	-140.96	-6.15	-33.84	-131.88	-11.39	-30.40	-123.62	-0.12	-22.71	-118.46

Herein, the conductor-like solvation model (COSMO) is used to include the effect of solvation quantitatively in the calculation.

**2. Solvation.** The treatment of solvation effects using self-consistent reaction field methods such as COSMO<sup>15</sup> have become widely available, and their ability to reproduce solvation energies, spectroscopic properties, and other solvation effects has been demonstrated.<sup>31</sup> In COSMO, the solute molecule is represented as a cavity in a dielectric continuum with the dielectric constant of the solvent. The polarization of the dielectric medium by the charge distribution of the solute is modeled by screening charges on the surface of the cavity. This procedure gives an electrostatic correction term to the Kohn-Sham eigenvalues. As mentioned above, outer-sphere processes, which include solvent reorganization as well as the specific interaction of the solvent with the complex, are not accounted for in COSMO. The main difference between COSMO and other self-consistent reaction field methods is that the solvent is treated as a perfect conductor. The result of this simplified model is then corrected by a simple scaling factor  $(\epsilon - 1)/(\epsilon + x)$ , where  $\epsilon$  is the dielectric constant of the solvent and  $x$  is an empirical scaling factor.

**2.1. COSMO Model.** For neutral **1-CH<sub>3</sub>**, the COSMO solvation model ( $\epsilon = 37.5$  for CH<sub>3</sub>CN) gives an electrostatic solvation energy of -11.3 kcal/mol (DMol), which increases to -40.0 and -141.0 kcal/mol for the mono- and dianionic forms, respectively (Table 3). Table 4 summarizes the impact of solvation on the geometry. The geometry optimization including the COSMO correction results in only small structural changes even for the dianionic species, which show the largest solvation energy. In general, solvation gives rise to a contraction of the Fe-Fe bond since the excess charge causing a structural expansion is stabilized to some extent by the COSMO charges on the solute surface. Solvation has a very pronounced effect on the energies of charged species, and smaller corrections for the neutral solutes are calculated. The binding energy term of the disproportionation reaction energy calculated using eq 8 indicates that the disproportionation reaction is downhill for both [**1-CH<sub>3</sub>**]<sup>-</sup> and [**1-CF<sub>3</sub>**]<sup>-</sup> (Table 5).<sup>32</sup> ADF and DMol results for

**Table 4.** Impact of COSMO on the Structure. Difference in Bond Length (Å) and Flap Angle (deg)

	neutral	monoanion	dianion
DMol, <b>1-CH<sub>3</sub></b>			
Fe-Fe	-0.014	-0.047	-0.027
av Fe-P	0.015	0.009	0.005
P-P'	0.025	0.050	0.048
flap angle	-1.1	-2.4	0.9
DMol, <b>1-CF<sub>3</sub></b>			
Fe-Fe	0.003	-0.017	-0.018
av Fe-P	-0.005	-0.006	-0.006
P-P'	-0.011	0.009	0.001
flap angle	0.4	0.4	0.0
ADF, <b>1-CH<sub>3</sub></b>			
Fe-Fe	-0.003	-0.013	-0.022
av Fe-P	0.011	0.005	0.000
P-P'	0.009	0.017	0.030
flap angle	-1.2	-1.0	0.44
ADF, <b>1-CF<sub>3</sub></b>			
Fe-Fe	-0.016	-0.002	-0.009
av Fe-P	-0.015	-0.002	-0.004
P-P'	-0.023	-0.001	0.003
flap angle	0.2	0.1	0.0

**Table 5.** Binding Energy Differences of the COSMO Anions, in eV

	(1-) → (0)	(1-) → (2-)	total
DMol, <b>1-CH<sub>3</sub></b>	2.88	-3.32	-0.44
DMol, <b>1-CF<sub>3</sub></b>	3.89	-4.21	-0.32
ADF, <b>1-CH<sub>3</sub></b>	2.93	-3.16	-0.23
ADF, <b>1-CF<sub>3</sub></b>	3.87	-4.39	-0.53

the energies of the disproportionation reaction are in very good agreement.

It is noteworthy that the ADF solvation energy for **1-CF<sub>3</sub>** is obviously too low. The calculated electrostatic solvation energy for the neutral species of -0.1 kcal/mol is too small compared to a typical value of roughly -10 kcal/mol, as observed in the DMol calculation for **1-CF<sub>3</sub>** of -11.4 kcal/mol. The use of unoptimized radii for the atoms is most likely the cause for this inconsistency. The COSMO calculations on neutral systems are expected to be most sensitive to the wrong choice of radii,<sup>15c</sup> so that the ADF solvation energies for the anionic species ([**1-CF<sub>3</sub>**]<sup>-</sup>, -22.7 kcal/mol; [**1-CF<sub>3</sub>**]<sup>2-</sup>, -118.5 kcal/mol) are very reasonable despite the poor quality of the radii.

**2.2. Hirshfeld Charge Distribution Analysis.** An understanding of how the added charge is distributed throughout the molecule is an important issue to address since it is anticipated

(31) (a) Baldrige, K. Klamt, A. *J. Chem. Phys.* **1995**, *106*, 6622. (b) Truong, T. N.; Stefanovich, E. V. *J. Chem. Phys.* **1995**, *103*, 3709. (c) Klamt, A.; Jonas, V. *J. Chem. Phys.* **1996**, *105*, 9972. (d) Ridley, J.; Zerner, M. C. *Theor. Chim. Acta* **1976**, *42*, 223. (e) Zerner, M. C.; Loew, G. H.; Kirchner, R. F.; Mueller-Westerhoff, U. *J. Am. Chem. Soc.* **1980**, *102*, 589. (f) Tomasi, J.; Persico, M. *Chem. Rev.* **1994**, *94*, 2027.

(32) The disproportionation energy,  $\Delta\Delta E$ , of -0.22 eV in acetonitrile solvent ( $\epsilon = 37.5$ ) increases to +0.08 eV in CH<sub>2</sub>Cl<sub>2</sub> solvent ( $\epsilon = 9.08$ ). As expected, the lower dielectric constant solvent gives rise to a smaller disproportionation constant due to the greater decrease in the energy of the A(1-) → A(2-) half-reaction relative to the A(1-) → A(0) half-reaction.



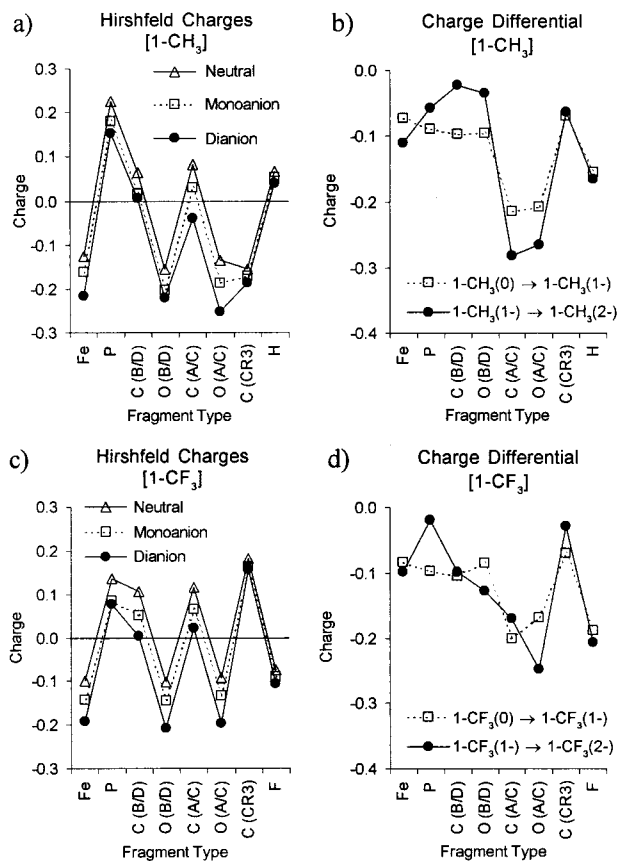


**Figure 3.** Hirshfeld charges averaged by atom type from the calculations on the ionic forms of **1-CH<sub>3</sub>** and **1-CF<sub>3</sub>** including solvation (DMol results).

that this distribution may play a role in dictating the observed redox behavior. Formally, the iron centers are reduced from the oxidation state I<sup>+</sup> in the neutral complex to 0 in the dianion. It is anticipated that the carbonyl ligands will play an important role in the distribution of the excess charge. The Hirshfeld charge analysis<sup>33</sup> allows a quantitative evaluation of the charge distribution pattern.

It is convenient to group chemically equivalent fragments of the molecule, for which the same formal charge is expected. In the neutral and monoanionic forms, carbonyl groups at positions A and B (Table 1) are structurally related, and identical charge distributions are expected. Similarly, two symmetry-inequivalent sites for the carbonyl ligands are observed in the dianion: the out-of-plane (C) and in-plane (D) sites. The two iron and two phosphorus atoms are expected to have the same partial charges, respectively. The absolute Hirshfeld charges averaged for symmetry-equivalent fragment types are shown in Figure 3a and c for **1-CH<sub>3</sub>** and **1-CF<sub>3</sub>**, respectively. To illustrate the changes of charge distribution with each additional electron, charge differential plots are prepared (Figure 3b,d). Charge differences of each fragment for the reduction steps have been added, so that the total fraction of charge being added to the fragment type could be displayed. The graph therefore integrates to the charge of one electron for each step. The labels A/B (neutral/monoanion) and C/D (dianion) have been grouped together, since the number of carbonyls in the positions A/B (4) and C/D (2) are equal; they are, however, not chemically equivalent. The ADF and DMol results show nearly identical charge distributions; therefore, only DMol values are shown in Figure 3.

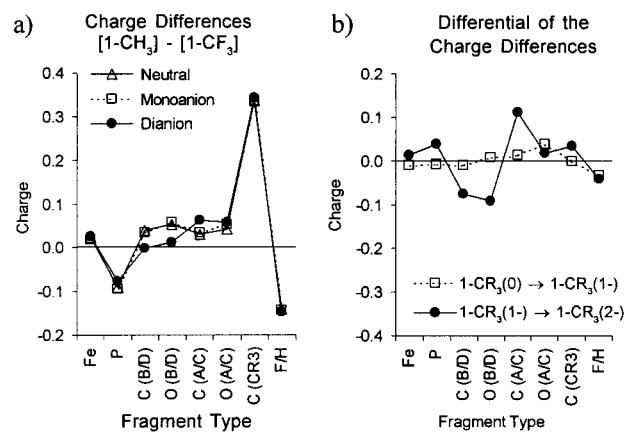


**Figure 4.** Hirshfeld charge change from replacing CH<sub>3</sub> by CF<sub>3</sub> (DMol results).

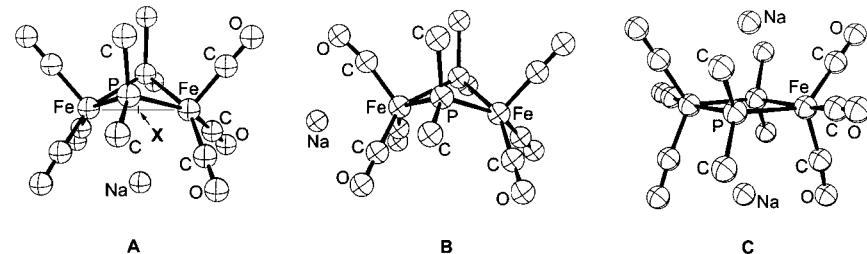
**2.2.1. 1-CH<sub>3</sub>.** The carbonyl oxygens carry the largest overall negative charge in the neutral species. The largest positive charge is assigned to phosphorus. It is noteworthy that the absolute value of the Hirshfeld charge on iron, which is assigned a formal oxidation number of I<sup>+</sup>, is slightly negative (−0.13). The stepwise reduction of iron to a formal oxidation state of 0 in the dianion is accompanied by an increased negative charge (−0.23). The overall charge distribution pattern is conserved in both steps. Surprisingly, the significant structural change does not give rise to a dramatic charge redistribution, as indicated by the similarity of the three graphs in Figure 3a.

The differential plot (Figure 3b) highlights the distribution of the additional charge quantitatively. As expected, the carbonyl ligands do play the most important role in accepting the excess charge. Roughly 60–70% of the additional charge is distributed among the carbonyl groups. Carbon and oxygen are involved in the charge dissipation to the same extent, and about 10% of the total charge is distributed to each carbonyl group. The in-plane position for the CO group in the dianion (position D) seems to display charge saturation at −0.2, which is reached after the first reduction (position B); the second charge does not lead to any additional change at that CO fragment. More than 55% of the second charge is distributed to the carbonyl ligands in the C position. Interestingly, the charges on the C and H of the methyl group are essentially invariant over the course of the redox reaction. The 12 hydrogens accommodate a total charge of roughly −0.15.

The charge on the bridging phosphorus shows only a small change upon reduction, indicating that the bridging ligand does not participate actively in the charge redistribution. The change is even smaller for the second electron, which is in good agreement with the composition of the frontier orbital accepting the electron. The phosphorus character in the LUMO of the neutral, SOMO (singly occupied molecular orbital) of the monoanion, and HOMO of the dianion decreases with increasing degree of Fe–P core planarity and is essentially zero in the planar dianion.

**2.2.2. 1-CF<sub>3</sub>.** Exchange of the methyl ligands by trifluoromethyl groups has a large effect on the absolute values of the Hirshfeld charges. Figure 4a shows the formal charge differences of equivalent sites between **1-CH<sub>3</sub>** and **1-CF<sub>3</sub>**. The differential of the charge differential upon reduction with respect to the equivalent site between the two derivatives allows a convenient assessment of the effect that the structural variation has to the charge distribution. This double differential plot is shown in Figure 4b. The largest change in charge is observed at the CR<sub>3</sub> carbon site illustrated by a charge differential of +0.34 in Figure

(33) Hirshfeld, F. L. *Theor. Chim. Acta B* **1977**, *44*, 129.

**Table 6.** Ion Pair Calculation in the Gas Phase on **1-CH<sub>3</sub>**


	DMol	DMol	DMol	DMol	DMol	DMol	DMol	ADF	ADF	ADF	ADF	ADF	ADF	ADF
anion charge	-1	-2	-1	-1	-2	-1	-2	-1	-2	-1	-1	-2	-1	-2
countercation	Li	Li	Na	Na	Na	K	K	Li	Li	Na	Na	Na	K	K
structure	A	C	B	A	C	A	C	A	C	B	A	C	A	C
Fe-Fe/Å	3.157	3.544	3.189	3.155	3.602	3.187	3.609	3.167	3.548	3.265	3.182	3.602	3.200	3.624
Fe-P/Å	2.290	2.332	2.315	2.296	2.331	2.289	2.327	2.296	2.342	2.312	2.297	2.336	2.296	2.337
Fe-P'/Å	2.290	2.301	2.261	2.296	2.299	2.289	2.302	2.296	2.305	2.269	2.297	2.308	2.296	2.304
P-P'/Å	2.933	2.984	2.903	2.931	2.913	2.901	2.899	2.933	2.999	2.904	2.908	2.937	2.907	2.900
X-cation/Å	2.022	2.068		2.423	2.732	2.970	3.202	2.012	2.066		2.417	2.725	2.963	3.189
X-cation'/Å		2.048			2.528		3.180		2.041			2.519		3.171
flap angle <sup>17</sup> /deg	127.7	175.9	128.7	126.3	177.7	128.2	178.8	127.4	175.7	134.4	127.0	178.0	128.4	179.0
Fe-P-Fe/deg	87.2	99.7	77.7/79.9	86.8	102.0	88.2	102.4	87.2	99.5	90.9	87.7	101.6	88.4	102.6
P-Fe-P/deg	79.7	80.1	88.3	79.3	77.9	78.6	77.5	79.4	80.3	77.8/79.6	78.5	78.4	78.5	77.3
C-P-C/deg	98.7	95.6	97.8	98.3	92.3	97.5	91.1	98.5	95.5	98.2	97.7	92.3	97.6	90.7
Hirshfeld charge of [M]	0.356	0.291	0.600	0.477	0.450	0.559	0.540	0.369	0.309	0.581	0.469	0.447	0.574	0.561
E(binding)/eV	-155.36	-157.26	-154.35	-154.87	-156.04	-155.14	-156.60	-207.38	-209.65	-206.28	-206.87	-208.46	-206.97	-208.72
E(LUMO)/eV	-2.68	-2.77	-2.50	-2.49	-2.48	-2.28	-2.12	-2.32	-2.58	-2.85	-2.13	-2.21	-1.96	-1.86
E(HOMO)/eV	-4.21	-5.18	-4.33	-3.94	-4.78	-3.79	-4.45	-3.94	-4.50	-3.49	-3.69	-4.52	-3.54	-4.17

4a. In **1-CH<sub>3</sub>** a negative Hirshfeld charge of  $-0.15$  is assigned to the carbon, whereas the charge at hydrogen is  $+0.18$ . The expected effect of replacing hydrogen with a highly electronegative fluorine changes the CR<sub>3</sub> group from electron-donating (R = H) to electron-withdrawing (R = F). The total fragment charge of the CR<sub>3</sub> group is  $+0.19$  and  $-0.17$  for the CH<sub>3</sub> and CF<sub>3</sub> functional groups, respectively. The phosphorus atom is less positively charged in **1-CF<sub>3</sub>** (0.14) than in **1-CH<sub>3</sub>** (0.23), indicating that the phosphido group is a better electron acceptor in the CF<sub>3</sub>-substituted analogue. Accordingly, the P(CF<sub>3</sub>)<sub>2</sub> ligand gives rise to a smaller negative charge on the carbonyl ligands in [**1-CF<sub>3</sub>**]<sup>2-</sup> than in [**1-CH<sub>3</sub>**]<sup>2-</sup>.

The electronic perturbation caused by the CR<sub>3</sub> group is constant over the 2 e<sup>-</sup> redox process. For both **1-CH<sub>3</sub>** and **1-CF<sub>3</sub>**, the CR<sub>3</sub> groups accept roughly 30% of the charge in each step. The double differential plot of the charges in Figure 4b illustrates the difference of charge distribution caused by replacing hydrogen with fluorine. The flat curve around the zero line for the first step indicates no significant changes of the charge distribution scheme, which is in good agreement with the small contribution of the P(CR<sub>3</sub>)<sub>2</sub> to the charge dissipation identified above. For the second reduction step, the carbonyl sites in the two derivatives show different charge-accepting abilities.

**3. Ion Pair Models.** Like solvation, the addition of counterions to the monoanionic and dianionic species serves as a means for compensating the negative charge. Ion pair calculations have been carried out for the **1-CH<sub>3</sub>** series.<sup>34</sup> There are two possible sites for the ion pair formation. Arguments based on the Fukui(-) function<sup>35</sup> would suggest that the partially

elongated Fe-Fe bond, where most of the HOMO-based electron density is located, is the most likely site to add the counterion (Table 6, structure A). Chemical intuition as well as Hirshfeld charge analysis would give preference to the carbonyl oxygen sites that carry the highest negative charge and are more accessible than the Fe-Fe bond (Table 6, structure B). Geometry optimizations for these two possible structures reveal that the ion pair structure A is more stable. The binding energy is roughly 0.5 eV lower in both DMol and ADF calculations.

The structural changes of the complex in the ion pair in comparison to the gas phase are relatively small (Table 6) for [**1-CH<sub>3</sub>**]<sup>2-</sup>. The Fe-Fe distance decreases by approximately 0.1 Å compared to the ionic gas-phase calculation due to the partial removal of electron density from the Fe-Fe antibonding HOMO by the counterion. The same mechanism of charge dissipation leads to a more pronounced difference in the dianionic form of the complex, where Li<sup>+</sup> shows the largest effect. The Fe-Fe distance in the [Li]<sub>2</sub>[**1-CH<sub>3</sub>**] ion pair is 3.55 Å, which is 0.19 Å shorter than that in the gas-phase dianion. The distance of the counterion to the midpoint of the Fe-Fe axis X (Table 6) shows a linear correlation with the ionic radii of Li, Na, and K ions in six-coordinated crystals (Figure 5a).<sup>36</sup> The smaller positive charges on the cation in the dianionic ion pairs, [M]<sub>2</sub>[**1-CH<sub>3</sub>**], give rise to a larger cation, so the average distances from the Fe-Fe center is larger.

**3.1. Hirshfeld Charge Analysis as a Function of Counterion.** The formal charges of the counterions define how much of the negative charge resides on the anion. The charge on the cation increases from  $+0.36/+0.30$  (monoanion/dianion, Li) to  $+0.47/+0.44$  (monoanion/dianion, Na), to  $+0.56/+0.51$  (monoanion/dianion, K). The Hirshfeld charge of the cation is plotted as a function of the electronegativity of the counterion (Figure 5b). A linear extrapolation using the Na and K points predicts a more positive formal charge for Li than is observed.

(34) The ion pair formation for **1-CF<sub>3</sub>** is more difficult to treat since the steric demands of the CF<sub>3</sub> fragments lead to unfavorable interactions with the cation, especially in the dianionic form. In addition, the HOMO is sterically shielded and is not easily exposed to a direct electrophilic attack. A different ion pairing strategy than that applied here for **1-CH<sub>3</sub>** is therefore necessary.

(35) (a) Fukui, K. *Science* **1987**, *218*, 747. (b) Fukui, K.; Yonezawa, T.; Shingu, H. *J. Chem. Phys.* **1952**, *20*, 722.

(36) Shannon, R. D. *Acta Crystallogr.* **1974**, *A32*, 751.



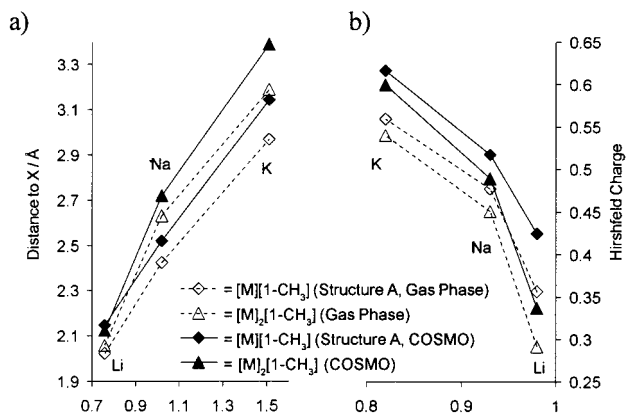


**Figure 5.** (a) Distance of the counteranion from the midpoint of the Fe–Fe vector as a function of ionic radius (DMol results). (b) Correlation of the counteranion Hirshfeld charge with Pauling electronegativity (DMol results).

The magnitude of the formal charge on Li is only slightly more positive than charges assigned to other atoms of the anionic molecule, which are covalently bound to each other (Figure 6), consistent with the expectation that the interaction of lithium with the anion is the most covalent interaction in the cation series. The averaged charges of the cations in the dianionic ion pairs are lower than those of the monoanionic systems, implying that the electron-donating ability of the dianion is more than twice that of the monoanion. Furthermore, the charge differences of the counteranions between the monoanionic and dianionic systems increase consistently in the series K, Na, and Li. The electron affinity of a molecular anion is a nontrivial property that will depend on a variety of parameters, such as charge and geometry of the molecule.

The charge distribution scheme of the anion fragments, [1-CH<sub>3</sub>]<sup>-</sup> and [1-CH<sub>3</sub>]<sup>2-</sup>, in the ion pairs (Figure 6) indicates a slightly different dissipation pattern than seen for the COSMO model. The magnitude of the change in charge upon reduction for both steps is decreased due to the presence of the electron-withdrawing cation. The total charge to be distributed in the anion increases from  $-0.36/-0.60$  (monoanion/dianion) in the Li ion pair to  $-0.56/-1.02$  (monoanion/dianion) in the K ion pair. Accordingly, the magnitude of the changes in charge increases down the period in the differential plot (Figure 6b,d,f), but the general pattern of charge dissipation is very similar for all three counterions. In contrast to the COSMO model, the bridging phosphido ligand plays a major role in accepting the added charge in the second reduction step for the ion pair models, effectively competing with the carbonyl ligands. In the Li ion pair, phosphorus accepts as much charge as a carbonyl carbon (Figure 6b). The accepting ability of phosphorus decreases down the period as the charge density of the cation decreases, and the total negative charge on the anion increases. Presumably the close contact distance between the cation and the bridge in the structure of the dianion plays a role in modulating the accepting ability of phosphorus (Table 7, structure C). In the K ion pair the electron-accepting role of the bridge has reached approximately the level of the free anion (Figure 6f). The overall picture that emerges from this analysis is that the Li ion pair is best characterized as a part of the molecule with strong electronic interaction with the anionic fragment, whereas the Na and K ion pairs are best described as classical contact ion pairs.

**3.2. Disproportionation Energies.** Remarkably, the calculation of  $\Delta\Delta E$  according to eq 8 gives negative values for the total energy change in all cases (Table 7), indicating that the

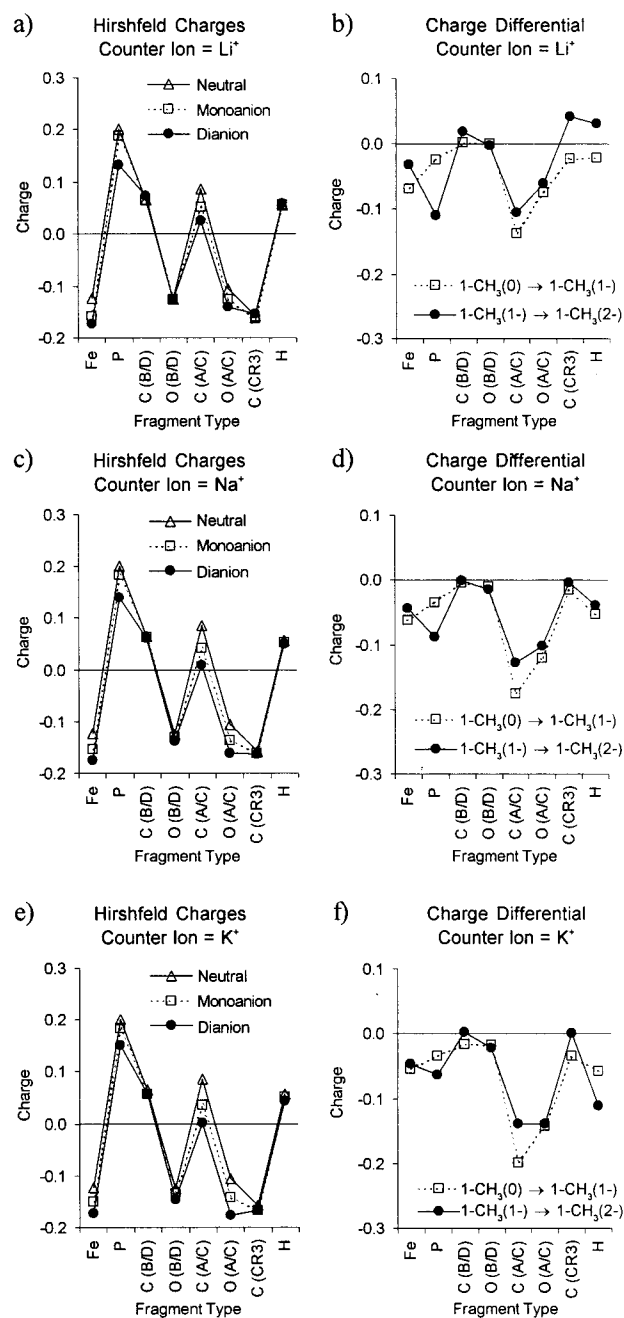


**Figure 6.** Hirshfeld charges of the ion pair complexes with solvation (DMol results).

**Table 7.** Binding Energy Differences of the Ion Pairs [M]<sub>n</sub>[1-CH<sub>3</sub>], in eV

	(1-) → (0)	(1-) → (2-)	total
DMol, Li	1.38	-1.90	-0.52
DMol, Na	0.89	-1.18	-0.29
DMol, K	1.16	-1.45	-0.29
ADF, Li	1.84	-2.27	-0.43
ADF, Na	1.33	-1.58	-0.25
ADF, K	1.43	-1.75	-0.32

disproportionation (eq 2) including counterions is energetically downhill. The qualitative difference between lithium and the other counterions is demonstrated in the relative energy differences. The covalency of the interaction of Li<sup>+</sup> with the dianion pushes the energetic difference between the mono- and dianion further apart, so that the half-reaction A(1-) → A(2-), for

**Table 8.** Ion Pair Calculation with COSMO on **1-CH<sub>3</sub>**

	DMol	DMol	DMol	DMol	DMol	DMol	DMol	ADF	ADF	ADF	ADF	ADF
anion charge	-1	-2	-1	-2	-1	-2	-1	-2	-1	-2	-1	-2
countercation	Li	Li	Na	Na	K	K	Li	Li	Na	Na	K	K
Fe-Fe'/Å	3.156	3.577	3.177	3.611	3.177	3.636	3.154	3.548	3.221	3.610	3.239	3.646
Fe-P/Å	2.295	2.337	2.300	2.337	2.290	2.317	2.292	2.340	2.298	2.346	2.295	2.332
Fe-P'/Å	2.295	2.307	2.300	2.312	2.290	2.301	2.292	2.301	2.298	2.313	2.290	2.311
P-P'/Å	2.952	2.959	2.917	2.929	2.916	2.848	2.927	2.988	2.912	2.947	2.902	2.875
X-cation/Å	2.147	2.168	2.519	2.841	3.143	3.414	2.080	2.120	2.472	2.792	3.017	3.180
X-cation'/Å		2.077		2.598		3.367		2.073		2.579		3.157
flap angle <sup>17</sup> /deg	127.7	175.3	126.6	177.7	128.1	179.8	126.8	175.3	129.9	179.8	131.5	179.9
Fe-P-Fe/deg	86.9	100.7	87.4	101.9	87.8	103.8	86.9	99.7	89.0	101.5	89.8	103.5
P-Fe-P/deg	80.0	79.1	78.7	78.0	79.1	76.1	79.4	80.2	78.6	78.4	78.5	76.5
C-P-C/deg	99.3	97.4	98.3	93.5	98.3	95.3	98.3	95.6	98.0	93.1	97.9	93.1
Hirshfeld charge of [M]	0.424	0.337	0.517	0.489	0.616	0.599	0.407	0.333	0.508	0.476	0.608	0.573
E(binding)/eV	-156.41	-158.51	-155.49	-156.89	-155.82	-157.70	-207.56	-209.90	-207.08	-208.93	-207.13	-209.01
E(LUMO)/eV	-2.40	-2.55	-2.39	-2.44	-2.23	-2.22	-2.25	-2.51	-2.23	-2.37	-2.06	-2.06
E(HOMO)/eV	-3.88	-4.97	-3.81	-4.75	-3.71	-4.53	-3.82	-4.93	-3.79	-4.63	-3.70	-4.375
electrostatic $E_{\text{sol}}/$ kcal mol <sup>-1</sup>	-30.96	-40.76	-17.89	-26.34	-20.93	-32.75	-8.57	-10.04	-10.31	-18.18	-8.84	-10.09

which a relatively large  $\Delta E$  of  $-1.9$  eV (DMol) is calculated, determines the magnitude of  $\Delta\Delta E$ .

**3.3. Solvation of the Ion Pair.** The overall charge of the entire ion pair is always zero, so the solvation energies of the different ion pairs are expected to be approximately the same order of magnitude and relatively small in comparison to the values for  $[1-\text{CH}_3]^-$  and  $[1-\text{CH}_3]^{2-}$ . A small value for the solvation energy implies that the medium should give rise to only a small perturbation, which should result in only insignificant structural changes for the geometry with the COSMO corrections. Our results confirm this expectation (Table 8). The most pronounced difference in the calculated COSMO ion pair structures<sup>37</sup> in comparison to the gas-phase ion pair structures is an increase in the cation-anion distance. The charges of both ions are partially stabilized by screening charges on the COSMO surface, giving rise to a weaker interaction between the positive and negative particles. Accordingly, a higher formal charge polarization on the ions is expected in comparison to the gas phase. The Hirshfeld charges of the counterions show that the positive charges are, indeed, higher throughout the whole series in comparison to the gas-phase counterparts. The gas-phase charges of 0.36/0.29 (Li), 0.48/0.45 (Na), and 0.56/0.54 (K) increase to 0.42/0.34 (Li), 0.52/0.49 (Na), and 0.62/0.60 (K) for  $[M][1-\text{CH}_3]/[M]_2[1-\text{CH}_3]$ , respectively. The COSMO corrections therefore make the interaction of the cation with the complex anion more ionic. No qualitative differences in the charge distribution patterns of the complex anion due to the COSMO correction on the ion pairs are observed.

The lithium cation carries the smallest positive charge in the series of the three alkali cations; therefore, the smallest effect due to solvation might be expected for the Li ion pair on the basis of purely electrostatic arguments. However, the lithium ion pair shows the largest solvation energy in the series (Table 8), and the calculated solvation energy of  $[\text{Li}][1-\text{CH}_3]$  ( $-31.0$  kcal/mol) is roughly twice that of  $[\text{Na}][1-\text{CH}_3]$ . Two factors determine the solvation energy of a particle: the charge of the particle and its size. If the same amount of charge is distributed on a smaller surface, a larger solvation energy is expected. Figure 7a shows surface representations of the three ion pairs that are used to distribute the screening charges. Depending on

(37) Shorter cation-anion distances are consistently observed for ADF results in comparison with the DMol results, and the difference is largest for K ( $>0.2$  Å). This example illustrates the importance of the values for the parametrized COSMO radii. The resulting geometric variation in the anions is small, and the ADF energies are quite reasonable, confirming the trend in the DMol calculations for which optimized radii are available.

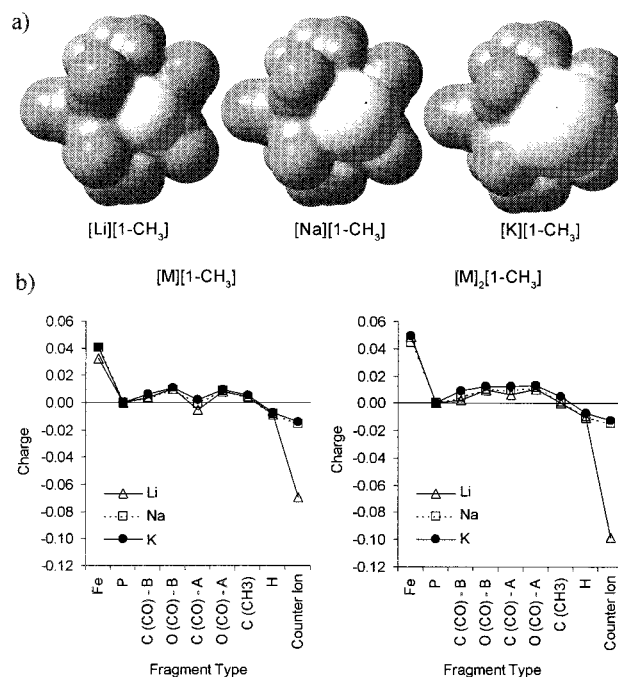


**Figure 7.** (a) Surfaces representing the ion pairs in solution. (b) DMol COSMO surface charge per unit area for  $[M][1-\text{CH}_3]$  (left) and  $[M]_2[1-\text{CH}_3]$  (right).

the fractional charges of the underlying atoms, charges of opposite sign are constructed on the COSMO surface, so that the polarized charges of the molecule are effectively compensated. Figure 7b shows the average of these screening COSMO charge densities (total charge per surface area) as a function of the atomic fragments. The COSMO surface of the counterion (light area in Figure 7a) is significantly smaller in the Li case compared to those for the other ion pairs, which gives rise to a significantly larger negative charge density in Figure 7b. This charge density is responsible for the relatively large structural change observed for  $[\text{Li}][1-\text{CH}_3]$  and  $[\text{Li}]_2[1-\text{CH}_3]$ . The bridging ligand is entirely inside the cavity, so no surface area is assigned to phosphorus. By far the smallest surface area is assigned to iron, for which a relatively high COSMO charge density is indicated.

The binding energy differences, including solvation, between the three redox species increase in magnitude compared to the gas-phase energies, in accord with the expectation that the higher polarization as the reduction progresses should give rise to a

**Table 9.** Binding Energy Differences of the Ion Pairs  $[M]_n[1-CH_3]$  with COSMO, in eV

	(1-) → (0)	(1-) → (2-)	total
DMol, Li	1.96	-2.10	-0.15
DMol, Na	1.04	-1.40	-0.36
DMol, K	1.37	-1.88	-0.52
ADF, Li	1.97	-2.34	-0.36
ADF, Na	1.51	-1.85	-0.34
ADF, K	1.56	-1.88	-0.32

**Table 10.** Ion Pair Formation Energy for  $[M]_n[1-CH_3]$  with COSMO, in kcal/mol (DMol)

	$[M][1-CH_3]$	$[M]_2[1-CH_3]$
Li	6.6	16.0
Na	-10.9	-24.3
K	-3.1	-12.7

larger contribution of solvation to the total energy. The total energy balance for the disproportionation reaction (eq 2) indicates that the disproportionation reaction is energetically downhill for all cations. The high COSMO stabilization of the  $[Li][1-CH_3]$  pair results in a decreased energy difference between the singly and doubly reduced species, giving a smaller  $\Delta\Delta E$  for the Li ion pair in comparison to the gas-phase value (Table 9). Solvation has the opposite effect on the relative energies of the Na and K ion pairs. The additional stabilization of the  $[M]_2[1-CH_3]$  gives rise to a more negative  $\Delta\Delta E$ . The COSMO surface charges for the sodium and potassium cation fragments are very similar. The potassium ion is significantly larger in size, so a larger total charge is screened on the potassium ion surface, resulting in a larger solvation energy (Table 8). The calculated binding energy differences for the Na and K ion pairs of  $-0.36$  and  $-0.52$  eV, respectively, are very close to the  $\Delta\Delta E$  calculated for the COSMO-stabilized ions of  $-0.44$  eV. Even though the formation of ion pairs has a large effect on the stability of the anions, the relative stabilities of the different redox species are very similar. The formation of ion pairs in which the nature of the interaction between the cation and the anion is primarily electrostatic does not affect the overall disproportionation reaction drastically. A counterion that binds to the anion in a more covalent fashion, such as lithium, is a serious perturbation of the electronic structure of the anion, and the impact is less predictable.

It is important to consider the energy of the ion pair formation reaction to evaluate the importance of the ion pairs in the reaction chemistry. This energy is evaluated by subtracting the sum of total energies of the solvated cation and anionic species from total energy of the solvated ion pair.

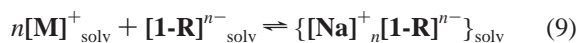
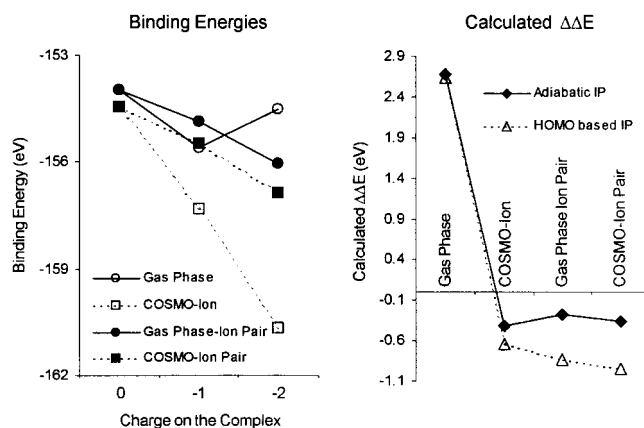


Table 10 summarizes the energies of ion pair formation in solution. The formation of the Li ion pair is energetically uphill by  $+6.6$  kcal/mol for  $[Li][1-CH_3]$  and  $+16.0$  kcal/mol for  $[Li]_2[1-CH_3]$ , whereas the ion pair is energetically downhill for the Na and K counterions by  $-10.9$  (Na)/ $-3.1$  (K) kcal/mol for  $[M][1-CH_3]$  and  $-24.3$  (Na)/ $-12.7$  (K) kcal/mol for  $[M]_2[1-CH_3]$ . The solvated ion pair model is the most realistic scenario for the electrochemical reaction in solution. This model predicts the existence of solvent-separated ions if Li is the counterion. The high solvation energy for the free lithium ion is the dominant factor contributing to the energy of ion pair formation.

**Figure 8.** (a) Comparison of DMol binding energies of  $[1-CH_3]^{n-}$  for gas-phase, COSMO ion, gas-phase ion pair, and COSMO ion pair models. Sodium results are plotted for ion pair calculations. (b) A comparison of  $\Delta\Delta E$  values for all four models and  $\Delta\Delta E$  values calculated based on the HOMO energy.

**HOMO Energy Correlation.** Zhao and Parr,<sup>38a,b</sup> Baerends and co-workers,<sup>38c-e</sup> Ziegler and Rauk,<sup>38f-h</sup> and recently Stowasser and Hoffmann<sup>38i</sup> have argued that Kohn–Sham orbitals can be used for chemical interpretation in a manner analogous to that for traditional molecular orbitals. We have analyzed our DFT results below in terms of approximate models proposed for redox reactions by Sarapu and Fenske,<sup>39a</sup> Bursten et al.,<sup>39b,c</sup> and others<sup>39d,e</sup> that relate the oxidation potential of a molecule to the energy of the HOMO, and the reduction potential to the energy of the LUMO. For a series of closely related organometallic complexes, an excellent linear correlation has been observed between the HOMO energy and the oxidation potential.<sup>39a-c</sup> The relative oxidation potential differences of the complexes are approximated reasonably well by the relative differences of their HOMO energies in accord with Koopman's theorem. The single orbital approach of Koopman's theorem is intuitively not suited to understand the electrochemistry of complex molecules quantitatively. In addition to the effects of electronic relaxation due to configuration change, the structural change upon removal/addition of electrons influences the energy of the complex significantly. In fact, it is the coupling of the structural change to the electrochemistry that gives rise to multielectron redox behavior. It is anticipated that a successful theoretical treatment would need to involve calculation of the ionization potential for a fully adiabatic process.

The binding energies for the four models presented in this study are summarized in Figure 8a. The large solvation energy of the mono- and dianionic forms gives rise to a steep correlation line for the solvated COSMO ion model. The relatively constant solvation energy term for the ion pair systems shift the solvated neutral, monoanion, and dianion to lower energy by approximately the same amount in comparison to the corresponding gas-phase energy. Figure 8b compares the  $\Delta\Delta E$  values calculated on the basis of the binding energies of the molecule

(38) (a) Zhao, Q.; Parr, R. G. *Phys. Rev.* **1992**, *46A*, 2337. (b) Zhao, Q.; Parr, R. G. *J. Chem. Phys.* **1993**, *98*, 543. (c) Baerends, E. J.; Gritsenko, O. V. *J. Phys. Chem.* **1997**, *101*, 5383. (d) Bickelhaupt, F. M.; Baerends, E. J.; Ravenek, W. *Inorg. Chem.* **1990**, *29*, 350. (e) Rosa, A.; Baerends, E. J. *New J. Chem.* **1991**, *15*, 815. (f) Ziegler, T.; Rauk, A. *Inorg. Chem.* **1979**, *18*, 1558. (g) Ziegler, T.; Rauk, A. *Inorg. Chem.* **1979**, *18*, 1755. (h) Ziegler, T.; Rauk, A. *Theor. Chim. Acta* **1978**, *46*, 1. (i) Stowasser, R.; Hoffmann, R. *J. Am. Chem. Soc.* **1999**, *121*, 3414.

(39) (a) Sarapu, A. C.; Fenske, R. F. *Inorg. Chem.* **1975**, *14*, 247. (b) Bursten, B. E.; Green, M. R.; Katovic, V.; Lightner, D., Jr. *Inorg. Chem.* **1986**, *25*, 831. (c) Bursten, B. E. *J. Am. Chem. Soc.* **1982**, *104*, 1299. (d) Pickett, C. J.; Fletcher, D. *J. Organomet. Chem.* **1975**, *102*, 327. (e) Wimmer, F. K.; Snow, M. R.; Bond, A. M. *Inorg. Chem.* **1974**, *13*, 1617.



to the values obtained by approximating the oxidation potentials by the HOMO energies of the geometry-optimized mono- and dianionic complexes.<sup>40</sup> Therefore, the HOMO energies include COSMO and ion pair corrections (Na values are shown in Figure 8).

A comparison of the two methods of analysis indicates that the approximate model using only HOMO energies reproduces the sign of  $\Delta\Delta E$  in all four cases, and the Koopman's theorem model would therefore lead to the same qualitative conclusion as our analysis scheme: that is, the  $2 e^-$  redox process is energetically downhill for all cases except the gas-phase model. The gas-phase values obtained by using either approach are essentially identical. This result provides strong evidence for the qualitative validity of the approach proposed by Sarapu and Fenske and Bursten et al. if the correct geometries for the different oxidation states are used.

## Conclusions

We have performed gradient-corrected DFT calculations on all three oxidation states of two iron dinuclear complexes, which undergo a two-electron redox reaction. The relative energies of the three oxidation states have been utilized to construct an energy profile of the redox reaction. Hirshfeld charges on the atoms in the molecule provide a detailed picture of changes in the electron distribution upon stepwise reduction. The main conclusions of this work are the following:

(i) Inclusion of solvation and/or ion pair effects in the calculational model is crucial to correctly reproduce the experimentally observed energy profile that favors the disproportionation reaction of the singly reduced complex. The shortcomings of gas-phase calculations arise from not including these effects.

(ii) The carbonyl ligands play a major role in dissipating the charge introduced in each reduction step. The electron affinity

---

(40) Note that the latter procedure follows the approximation scheme suggested by Sarapu and Fenske and Bursten et al., where fully optimized geometries from the corresponding complexes are used.

of a particular carbonyl ligand is dictated by its location in the molecule. A comparison of the charge dissipation pattern for the first and second steps provides information about the changes in electron affinity of the individual atoms over the course of the reduction. The changes in charge are dictated by the character of the orbitals involved in the redox reaction.

(iii) The self-consistent reaction field (SCRF) method to treat solvation effects (COSMO) is well suited to model the changes in electronic structure arising from solvation. Generally, the inclusion of the COSMO correction results in significant corrections to the total energy and orbital energies, even though only small structural changes are observed.

(iv) The model that includes both a counteranion and solvation is energetically and chemically the most realistic model. The interaction of  $Li^+$  with the anion is more covalent than the interaction of  $Na^+$  and  $K^+$ , but the formation of the lithium ion pair is energetically uphill.

(v) Both DFT programs, DMol and ADF, used in our study deliver essentially the same results. The lack of optimized COSMO radii in ADF gives rise to inconsistent results in some of our calculations.

**Acknowledgment.** This work was supported in part by the National Science Foundation. M.-H.B. is a Cray fellow. M.-H.B. thanks Dr. Lee Bartolotti and Professors Robert G. Parr, Weitao Yang, and Evert J. Baerends for valuable discussions and comments. We gratefully acknowledge the North Carolina Supercomputing Center for providing computational time and technical assistance.

**Supporting Information Available:** Coordinates for optimized geometries of all calculations reported herein (Tables S1–S4) and calculated vibrational frequencies for the system,  $[Fe_2(CO)_6(\mu_2-PMe_2)_2]^{0/-2-}$  (Table S5) (PDF). This material is available free of charge via the Internet at <http://pubs.acs.org>.

JA993522R